A&A manuscript no.
(will be inserted by hand later)

Your thesaurus codes are:
09 (06.06.3; 02.13.2; 02.03.1; 02.20.1; 03.13.3)

ASTRONOMY AND ASTROPHYSICS
October 9, 2000

MHD consistent cellular automata (CA) models I: Basic features

H. Isliker[1], A. Anastasiadis[2], and L. Vlahos[1]

[1] Section of Astrophysics, Astronomy and Mechanics
Department of Physics, University of Thessaloniki
GR 54006 Thessaloniki, GREECE
isliker@helios.astro.auth.gr, vlahos@helios.astro.auth.gr

[2] Institute for Space Applications and Remote Sensing
National Observatory of Athens
GR 15236 Penteli, GREECE
anastasi@space.noa.gr

Received ...; accepted ...

Abstract. A set-up is introduced which can be superimposed onto the existing solar flare cellular automata (CA) models, and which specifies the interpretation of the model's variables. It extends the CA models, yielding the magnetic field, the current, and *** an approximation to *** the electric field, in a way that is consistent with Maxwell's and the MHD equations. Applications to several solar flare CA models during their natural state (self-organized criticality (SOC)) show, among others, that (1) the magnetic field exhibits *characteristic large-scale organization* over the entire modeled volume; (2) the magnitude of the current seems spatially dis-organized, with no obvious tendency towards large-scale structures or even local organization; (3) bursts occur at sites with increased current, and after a burst the current is relaxed; (4) by estimating the energy released in individual bursts with the use of the current as Ohmic dissipation, it turns out that the power-law distributions of the released energy persist. The CA models, extended with the set-up, can thus be considered as *models for energy-release through current-dissipation*. The concepts of power-law loading and anisotropic events (bursts) in CA models are generalized to 3–D vector-field models, and their effect on the magnetic field topology is demonstrated.

Key words: solar flares, cellular automata, MHD, nonlinear processes, chaos, turbulence

1. Introduction

Cellular automata (CA) models for solar flares are successful in explaining solar flare statistics (peak flux, total flux, and duration distributions; Lu & Hamilton 1991 (hereafter LH91); Lu et al. 1993; Vlahos et al. 1995; Georgoulis & Vlahos 1996, 1998; Galsgaard 1996). They simplify strongly the details of the involved physical processes, and achieve in this way to model large volumes with complex field topologies and a large number of events. On the other hand, MHD simulations give insight into the details of the local processes, they are limited, however, to modeling relatively small fractions of active regions, due to the lack of computing power, yielding thus poor statistics and difficulties in comparing results to observations (e.g. Mikic et al. 1989; Strauss 1993; Longcope & Sudan 1994; Einaudi et al. 1996; Galsgaard & Nordlund 1996; Hendrix & Van Hoven 1996; Dmitruk & Gomez 1998; Galtier & Pouquet 1998; Georgoulis et al. 1998; Einaudi & Velli 1999). The *global* MHD flare models are still in the state of rather qualitative flare scenarios.

The MHD and the CA approach to solar flares seem to have very little in common: The former are a set of partial differential equations, based on fluid-theory and Maxwell's equations, whereas the latter are a set of abstract evolution rules, based (in the case of solar flares) on the analogy to critical phenomena in (theoretical) sand-piles. The scope of this paper is to bridge the gap in-between these two approaches: the solar flare CA models are reinterpreted and extended so as (i) to make these models completely compatible with MHD and with Maxwell's equations, and so that (ii) all relevant MHD variables are made available (e.g. the current and the electric field, which so far were not available in CA models).

In an earlier paper (Isliker et al. 1998), we have analyzed the existing solar flare CA models for their soundness with MHD. We asked the question whether the fields in these CA models and the evolution rules can be interpreted in terms of MHD. It turned out that these models can indeed be interpreted as a particular way of implementing numerically the MHD equations. This fact is not trivial, since these models had been derived in quite close analogy to the sand-pile CA model of Bak et al. (1987 and 1988), with vague association of the model's variables with physical quantities. For instance, some authors (Lu et al. 1993) explicitly discuss the question whether their basic grid variable is the magnetic field or not, without reaching to a definite conclusion. Isliker et al. (1998) brought forth not only how the existing CA models are related to MHD and what simplifications are hidden, but also where they differ from or even violate the laws of MHD and Maxwell's equation. Important is the fact that though the existing CA models can be considered as a strongly simplified numerical solution of the (simplified) MHD equations, *they do not represent the discretized MHD equations*: the time-step and the spacing between two grid sites are not small (in a physical sense), but finite; they are a typical temporal and spatial scale of the diffusive processes involved (see Isliker et al. 1998).

From the point of view of MHD, the main shortcomings of the existing CA models are (Isliker et al. 1998): (1) There is no control over consistency with Maxwell's equations. Interpreting, for instance, the vector-field in the CA models as the magnetic field leads to the problem that the gradient of the field ($\nabla \boldsymbol{B}$) cannot be controlled. (2) Secondary quantities, such as currents, are not available, and they cannot be introduced in the straightforward way by replacing differential expressions by difference-expressions, since, as mentioned, the grid-size must be considered finite (see also App. B.1). This lack of knowing how to calculate derivatives made it also useless to interpret the primary vector-field in the CA models as the vector potential (to avoid the $\nabla \boldsymbol{B}$-problem), since $\boldsymbol{B}$ could not be derived. The physical interpretation of these CA models remained so far problematic.

There are two basically different ways of developing CA models for flares further: (i) Either one considers CA models *per se*, tries to change the existing models further or invent new ones, with the only aim of adjusting them to reproduce still better the observations, i.e. one makes them a tool the results of which explain and maybe predict observed properties of flares. In this approach, one has not to care about possible inconsistencies with MHD or even Maxwell's equations, the various components of the model are purely instrumentalistic. (ii) On the other hand, one may care about the physical identification and interpretation of the various components of the model, not just of its results, and one may want the CA model to become consistent with the other approach to solar flares, namely MHD. In the approach (ii), some of the freedom one has in constructing CA models will possibly be reduced, since there are more 'boundary conditions' to be fulfilled in the construction of the model: the observations must be reproduced and consistency with MHD has to be reached. (Trials to construct new CA models which are based on MHD and not on the sand-pile analogy were recently made by Einaudi & Velli (1999), MacPherson & MacKinnon (1999), Longcope and Noonan (2000), and Isliker et al. (2000a).)

Our aim is in-between these two alternatives: we construct a set-up which can be superimposed onto each classical solar flare CA model, and which makes the latter interpretable in a MHD-consistent way (by *classical* CA models we mean the models of LH91, Lu et al. 1993, Vlahos et al. 1995, Georgoulis & Vlahos 1996, 1998, Galsgaard 1996, and their modifications, which are based on the sand-pile analogy). The set-up thus specifies the physical interpretation of the grid-variables and allows the derivation of quantities such as currents etc. It does not interfere with the dynamics of the CA (unless wished): loading, redistributing (bursting), and the appearance of avalanches and self-organized criticality (SOC), if the latter are implied by the evolution rules, remain unchanged. The result is therefore still a CA model, with all the advantages of CA, namely that they are fast, that they model large spatial regions (and large events), and therewith that they yield good statistics. Since the set-up introduces all the relevant physical variables into the context of the CA models, it automatically leads to a better physical understanding of the CA models. It reveals which relevant plasma processes and in what form are actually implemented, and what the global flare scenario is the CA models imply. All this was more or less hidden so far in the abstract evolution rules. It leads also to the possibility to change the CA models (the rules) at the guide-line of MHD, if this should become desirable. Not least, the set-up opens a way for further comparison of the CA models to observations.

In Sec. 2, we introduce our set-up. Applying it to several CA models (Sec. 3), we will demonstrate the usefulness and some of the benefits such extended models (i.e. classical models extended with our set-up) provide over the classical CA models, and we will reveal basic physical features of the CA models. The potential of the extended models to explain more observational facts than the classical CA models is, among others, outlined in the conclusions (Sec. 5).

2. Introduction of the set-up

The set-up we propose can be superimposed onto solar flare CA models which use a 3–D grid and a basic 3–D vector grid-variable, say $\boldsymbol{A}$. The corresponding set of evolution rules is not changed. (With a few modifications, the set-up can also be superimposed onto CA models which use a scalar field in a planar grid, which our set-up necessarily interprets as slab geometry, as will become clear later.)

We introduce our model on the example of the solar flare CA model of LH91, which we summarize here in order to make the subsequent presentation more concrete:

2.1. Summary of the CA model of LH91

In the LH91 model, to each grid-site $\boldsymbol{x}_{ijk}$ of a 3–D cubic grid a 3–D vector $\boldsymbol{A}_{ijk}$ is assigned. Initially, $\boldsymbol{A}_{ijk}$ is set to $(1,1,1)^T$, everywhere. The system is then loaded with the repeated dropping of increments at randomly chosen sites $\boldsymbol{x}_{ijk}$ (one per time-step)

$$\boldsymbol{A}(t+1,\boldsymbol{x}_{ijk}) = \boldsymbol{A}(t,\boldsymbol{x}_{ijk}) + \delta\boldsymbol{A}(t,\boldsymbol{x}_{ijk}), \tag{1}$$

where $\delta\boldsymbol{A}(t,\boldsymbol{x}_{ijk})$ has all its components as random numbers uniformly distributed in $[-0.2, 0.8]$.

After each loading event, the system is checked for whether the local 'stress', defined as

$$d\boldsymbol{A}_{ijk} := \boldsymbol{A}_{ijk} - \frac{1}{6}\sum_{n.n.}\boldsymbol{A}_{n.n.}, \tag{2}$$

where the sum goes over the six nearest neighbours of the central point $\boldsymbol{x}_{ijk}$, exceeds a threshold A_{cr}, i.e. whether

$$|d\boldsymbol{A}_{ijk}| > A_{cr}, \tag{3}$$

where $A_{cr} = 7$ is used. If this is the case, the field in the neighbourhood of the critical site is redistributed according to

$$\boldsymbol{A}_{ijk} \longrightarrow \boldsymbol{A}_{ijk} - \frac{6}{7}d\boldsymbol{A}_{ijk} \tag{4}$$

for the central point, and

$$\boldsymbol{A}_{n.n.} \longrightarrow \boldsymbol{A}_{n.n.} + \frac{1}{7}d\boldsymbol{A}_{ijk} \tag{5}$$

for its six nearest neighbours. In such a redistribution event (burst), energy amounting to

$$E_{rel.}^{\mathrm{LH91}} = \frac{6}{7}|d\boldsymbol{A}_{ijk}|^2 \tag{6}$$

is assumed to be released. The grid is scanned again and again to search for second, third etc. generation bursts, until the system is nowhere critical anymore and returns to the loading phase (the details we apply concerning the temporal evolution of the model are given in App. A; they are not explicitly stated in LH91). The field outside the grid is held constant and assumed to be zero.

2.2. Our set-up

We turn now to introducing our set-up, starting with a specification: We interpret the vector $\boldsymbol{A}_{ijk}$ at the grid sites $\boldsymbol{x}_{ijk}$ to denote the local vector-field, $\boldsymbol{A}(\boldsymbol{x}_{ijk})$. Note that this was not specified in the classical CA models. Lu et al. (1993) for instance discuss this point: it might also have been thought of as a mean local field, i.e. the average over an elementary cell in the grid.

Guided by the idea that we want to assure $\nabla\boldsymbol{B} = 0$ for the magnetic field $\boldsymbol{B}$, which is most easily achieved by having the vector-potential $\boldsymbol{A}$ as the primary variable and letting $\boldsymbol{B}$ be the corresponding derivative of $\boldsymbol{A}$ ($\boldsymbol{B} = \nabla\wedge\boldsymbol{A}$), we furthermore assume that the grid variable $\boldsymbol{A}$ of the CA model is identical with the vector-potential.

The remaining and actually most basic problem then is to find an adequate way to calculate derivatives in the grid. In general, CA models assume that the grid-spacing is finite, which also holds for the CA model of LH91 (as shown in detail by Isliker et al. 1998), so that the most straightforward way of replacing differential expressions with difference expressions is not adequate (see the detailed discussion in App. B.1, below; Vassiliadis et al. (1998) suggested to interpret CA models as the straightforwardly discretized (simplified) MHD equations, which we find problematic for the reasons given in App. B.1, and we therefore do not follow this approach, here).

Consequently, one has to find a way of continuing the vector-field into the space in-between the grid-sites, which will allow to calculate derivatives. There is, of course, an infinite number of possibilities to do so, and the problem cannot have a unique solution. Adequate possibilities definitely include: a) continuation of $\boldsymbol{A}$ with the help of an equation (e.g. demanding the resulting $\boldsymbol{B}$-field to be potential or force-free); b) interpolation, either locally (in a neighbourhood), or globally (through the whole grid). Trying several methods, we concluded that 3–D cubic spline interpolation is particularly adequate to the problem since it has remarkable advantages over other methods (e.g. it does not introduce oscillations in-between grid-sites, which would strongly influence the values of the derivatives, and it well reproduces the derivatives of analytically prescribed primary fields). The process of evaluating different continuation methods we went through, as well as the comparison of spline interpolation to other continuation-methods are described in App. B.

The 3–D interpolation is performed as three subsequent 1–D interpolations in the three spatial directions (Press et al. 1992). For the 1–D splines, we assume natural boundaries (the second derivatives are zero at the boundaries). Moreover, since in the CA model of LH91 it is assumed that around the grid there is a zero field which is held constant (see Sec. 2.1), we enlarge the grid by one grid point in all directions to include this constant zero-layer explicitly, using it however only for the interpolation. In the interpolation, the derivatives at the grid-points are immediately given by the analytically differentiated interpolating polynomials.

With the help of this interpolation, the magnetic field $\boldsymbol{B}$ and the current $\boldsymbol{J}$ are calculated as derivatives of $\boldsymbol{A}$, according to the MHD prescription:

$$\boldsymbol{B} = \nabla\wedge\boldsymbol{A}, \tag{7}$$

$$\boldsymbol{J} = \frac{c}{4\pi}\nabla\wedge\boldsymbol{B}. \tag{8}$$

*** To determine the electric field $\boldsymbol{E}$, we make the assumption that under coronal conditions the MHD approach is in general valid, and that $\boldsymbol{E}$ is**

reasonably well approximated by Ohm's law in its simple form, * $\boldsymbol{E} = \eta \boldsymbol{J} - \frac{1}{c}\boldsymbol{v} \wedge \boldsymbol{B}$, with η the diffusivity and $\boldsymbol{v}$ the fluid velocity. Since the classical CA models use no velocity-field, our set-up can yield only the resistive part,

$$\boldsymbol{E} = \eta \boldsymbol{J}. \tag{9}$$

In applications such as to solar flares, where the interest is in current dissipation events, i.e. in events where η and $\boldsymbol{J}$ are strongly increased, Eq. (9) can be expected to be a good approximation to the electric field. Theoretically, the convective term in Ohm's law would in general yield just a low-intensity, background electric field.

Eq. (9) needs to be supplemented with a specification of the diffusivity η: Isliker et al. (1998) have shown that in the classical CA models the diffusivity adopts the values $\eta = 1$ at the unstable (bursting) sites, and $\eta = 0$ everywhere else. This specifies Eq. (9) completely.

Remark 1: It is worthwhile noting that, since spline interpolation has the property to be the least curved of all twice differentiable interpolating functions, the grid-size is a typical smallest-possible length-scale of field structures, or, if we would think the CA to model MHD turbulence, it is something like an average smallest possible eddy-size.

Remark 2: With our set-up, field lines are made available: the interpolation was introduced to define derivatives at the grid-sites, but it can as well be used to determine the vector-potential, and therewith the magnetic field and the current, in between the grid sites. However, it is important to note that this field in between the grid sites is not used for the time-evolution of the model, it merely allows to visualize the evolution in the standard way through field-lines, if wished so (second order derivatives in-between the grid-sites, if needed, would have to be done numerically, since else their numerical values would depend on the order in which the three 1–D interpolations are done).

Remark 3: * **In this paper, we do not change the rules of the classical CA models to which we apply our set-up — except for the definition of energy release (Sec. 3.1.3). Our aim here is to show the usefulness of the set-up and to give some results and reveal some aspects by extending published CA models. While the redistribution rules have in detail been shown to represent diffusion events and fit nicely into an MHD scenario (Isliker et al. 1998), the loading process is strongly simplified and poorly follows a reasonable flare scenario: For instance, the loading process acts independently everywhere in the simulation box, whereas according to a realistic flare scenario (see e.g. Parker 1993) disturbances should appear independently only on one boundary (the photosphere, due to random foot-point motions or newly appearing flux), and propagate then into the interior of the simulation box along the magnetic field lines.**

To translate such a realistic loading scenario into the language of CA models has not been undertaken, so-far.* We just note that it would be quite straightforward to introduce a velocity field into the CA models: e.g. Isliker et al. (2000a) propose a CA model which uses a velocity field for the loading phase, but this model does not fall into the category of classical CA models since it does not follow the sand-pile analogy and uses different, MHD based, evolution rules. We leave the problem of introducing a velocity field and a more physical loading process into the classical CA models for a future study. * **In Isliker et al. 2000b, we will — among others — analyze in details what this simplified loading process physically represents.***

3. Applications of our set-up

3.1. Application to the CA model of Lu & Hamilton (1991)

Our first application is to the CA model of LH91 (see Sec. 2.1). The LH91 model has a fairly long transient phase and reaches finally a stationary state, the so-called SOC (self-organized criticality) state, in which spatially spreading series of bursts (avalanches) appear, alternating with quiet loading phases. The LH91 model gives basically three results concerning flare statistics, namely the distributions of total energy, peak-flux and durations, which are all power-laws with slopes that are in good agreement with the observations (Lu et al. 1993, Bromund et al. 1995).

Superimposing our MHD-frame onto the LH91 model such as it stands does not change anyone of the three results, since at this first stage we are not interfering with the dynamics (i.e. the evolution rules). The set-up allows, however, to address several questions in MHD language: Our main aim in the subsequent applications is to demonstrate that the set-up indeed yields a new and consistent interpretation of CA-models, to illustrate the behaviour of the secondary variables (currents, magnetic fields), and to reveal major features of them. (In the subsequent runs, we use a grid of size $30 \times 30 \times 30$, as LH91 did to derive their main results.)

3.1.1. Global structures of the vector-fields

First, we turn to the question what the global fields (vector-potential, magnetic field, current) look like during the SOC state. Thereto, the temporal evolution of the model is stopped at an arbitrary time during SOC state (in a phase where there are no bursts, i.e. during loading), and the magnitude of the fields at a cut with fixed z-coordinate are shown as a function of the x- and y-coordinates in Fig. 1. $|\boldsymbol{A}(x, y, z = z_0)|$ obviously exhibits a large-scale organization over the whole grid, it forms a

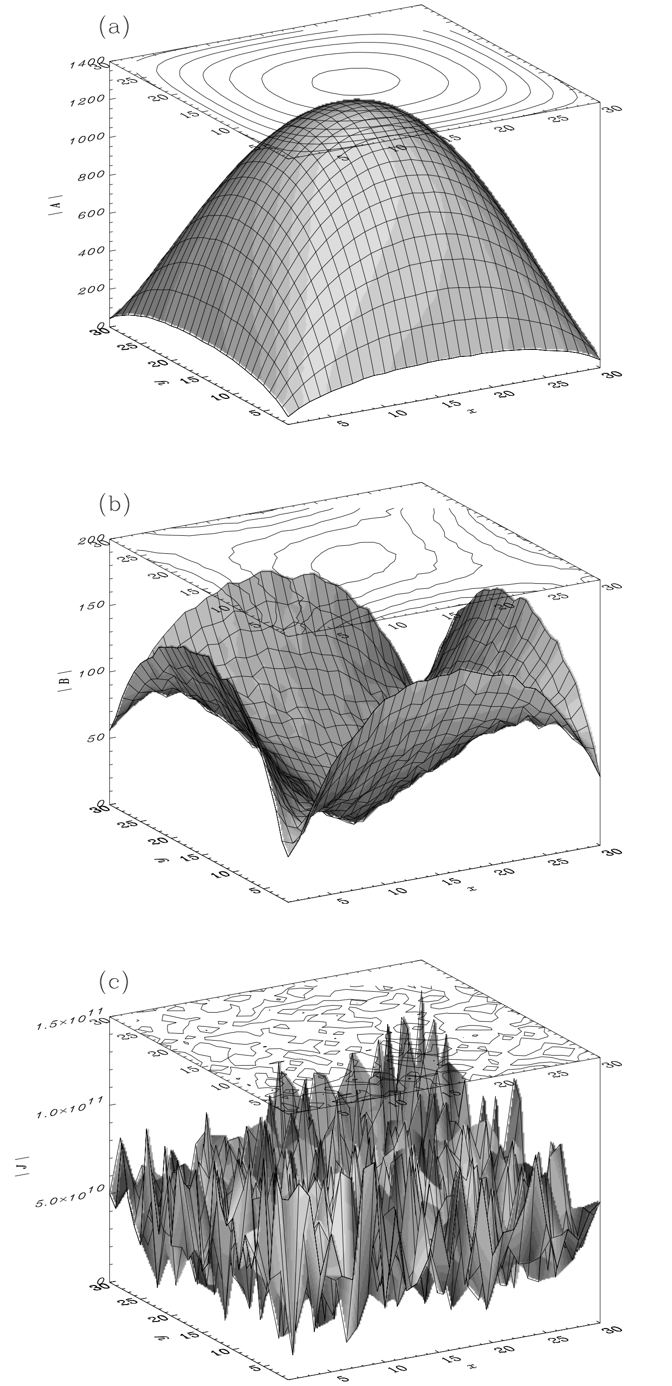

Fig. 1. Surface and contour plots of the magnitudes of (a) the vector-potential ($|\boldsymbol{A}|$), (b) the magnetic field ($|\boldsymbol{B}|$), and (c) the current ($|\boldsymbol{J}|$) as a function of x and y, for $z = 15$ fixed.

global convex surface (Fig. 1(a)). This convex surface has a slight random distortion over-lying, which visually cannot be discerned in Fig. 1(a), but becomes visible in the plot of $|\boldsymbol{B}|$ (Fig. 1(b)), the curl of $\boldsymbol{A}$, which still exhibits large-scale organization all over the grid, but is clearly wiggled. Finally, $|\boldsymbol{J}|$ shows no left-overs of a large scale organization anymore, it reflects the random disturbances of the convexity of $|\boldsymbol{A}|$ (Fig. 1(c)).

The large-scale structures shown in Fig. 1 are always maintained during the SOC state, neither loading nor bursting (and avalanches) destroy them, they just 'tremble' a little when such events occur. SOC state in the extended LH91 model thus implies large-scale organization of the vector-potential and the magnetic field, in the characteristic form of Fig. 1.

The large-scale organization of $\boldsymbol{A}$ is not an artificial result of our superimposed set-up, but already inherent in the classical LH91 model: in the classical LH91 CA model, there is only one variable, the one we call here $\boldsymbol{A}$, whose values are not affected by the interpolation we perform since it is the primary grid variable, so that Fig. 1(a) is true also for the classical, non-extended LH91 model.

*** The large scale structure for the primary grid-variable $|A|$ is the result of a combined effect: The preferred directionality of the loading increments (see Sec. 2.1) tries to increase $|A|$ throughout the grid. The redistribution events, which already in Bak et al. (1987; 1988) were termed diffusive events, and which in Isliker et al. (1998) were analytically shown to represent local, one-time-step diffusion processes, smooth out any too strong spatial unevenness of A, and they root the A-field down to the zero level at the open boundaries. The result is the convex surface of Fig. 1(a), blown-up from below through loading, tied to the zero-level at the edges, and forced to a maximum curvature which is limited by the local, threshold dependent diffusion events.**

As the SOC state, so is the large-scale structure independent of the concrete kind of loading, provided it fulfills the conditions that the loading increments exhibit a preferred directionality and are much smaller than the threshold (with symmetric loading, the SOC state is actually never reached, see LH91 and Lu et al. (1993)).

To make sure of the importance of the boundaries, we performed runs of the model with closed boundaries, and we found that neither a large-scale structure was developed in $|A|$, nor the SOC state was reached. *

3.1.2. Bursts

To illustrate the role of the current at unstable sites and during bursts, we plot in Fig. 2 the magnitude of the current before and after a typical burst: obviously, the current at the burst site $(x, y, z) = (20, 18, 3)$ has high intensity before the burst (Fig. 2(a)), and is relaxed after the burst (Fig. 2(b)). Inspecting a number of other bursts, we found that, generally, at sites where the LH91 instability criterion is fulfilled, the current is increased, too, and that bursts dissipate the currents. This is a first hint that clas-

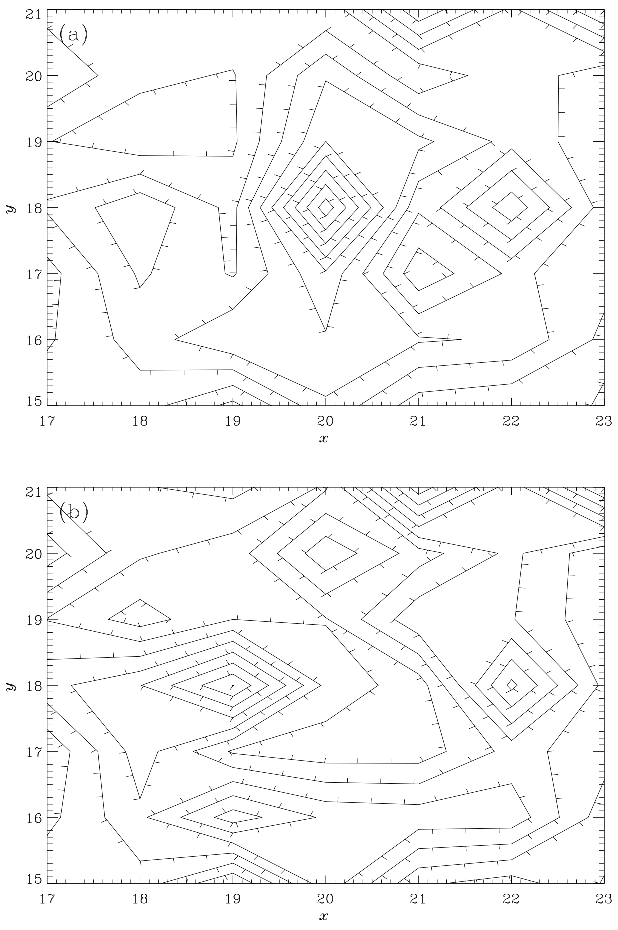

Fig. 2. The magnitude of the current ($|\boldsymbol{J}|$, contour-plot, with the ticks pointing 'downhill') as a function of x and y at a zoomed cut $z = 3$ through the grid, before (a) and after (b) a burst, which occurs in the middle of the plot, at $(x, y, z) = (20, 18, 3)$.

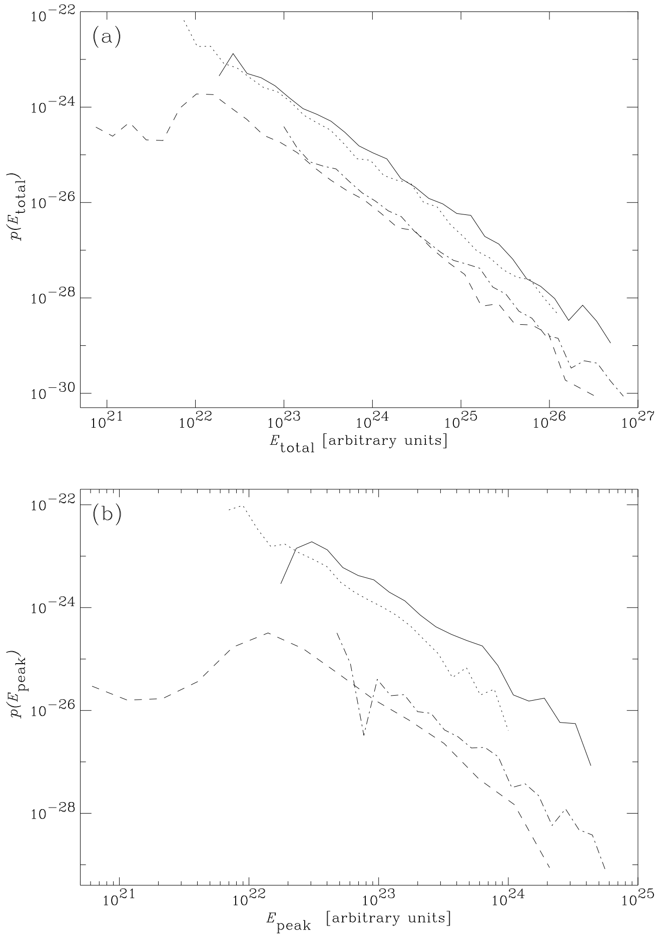

Fig. 3. The distribution of the total energy (a), and of the peak-flux (b), for different ways of measuring the released energy in a burst: $E_{burst} = \int dt \sum_{n.n.} \boldsymbol{J}(\boldsymbol{x}_{ijk})^2$ (solid); $E_{burst} = \int dt\, \boldsymbol{J}(\boldsymbol{x}_{ijk})^2$ (dotted); E_{burst} as the difference in $\sum_{n.n.} \boldsymbol{B}(\boldsymbol{x}_{ijk}, t)^2$ before and after the burst (dashed); $E_{burst} = \frac{6}{7} d\boldsymbol{A}^2$ (dash-dotted). (The distributions are normalized probability distributions, the last two were shifted in both directions for viewing them together with the first two.)

sical CA models can be interpreted as models for energy release through current-dissipation.

After the burst, at the neighbouring site $(21, 18, 3)$, the intensity of the current is increased, and indeed the presented burst gives rise to subsequent bursts, it is one event during an avalanche.

The magnetic field at the bursting site is reshaped, in a way which is difficult to interpret when using only the magnitude of it ($|\boldsymbol{B}|$) for visualization. May-be field line plots would help visualization, but we leave this for a future study.

3.1.3. Energy release and Ohmic dissipation

We now turn to the question what relation the energy release formula of LH91 (Eq. 6) has to the respective MHD relations: In parallel to using the formula of LH91, we determine the released energy in the following ways, closer to MHD: First, we assume it to be proportional to $\eta \boldsymbol{J}^2$ (with the diffusivity $\eta = 1$ at unstable sites, see Sec. 2.2), which we linearly interpolate between the two states before and after the burst. This is done in two ways, (i) summing over the local neighbourhood,

$$
\begin{aligned}
E_{burst}^{\int\sum J^2} &= \int_t^{t+1} \int_{n.n.} \eta\, \boldsymbol{J}(\boldsymbol{x}, t)^2 \, dt \, dV \approx \int_t^{t+1} \sum_{n.n.} \boldsymbol{J}_{n.n.}(t)^2 \, dt \\
&= \sum_{n.n.} \frac{1}{2} \left(\boldsymbol{J}^2_{n.n.;\, before} + \boldsymbol{J}^2_{n.n.;\, after} \right) \qquad (10)
\end{aligned}
$$

and (ii) without summing, but just taking into account the current at the central point,

$$
\begin{aligned}
E_{burst}^{\int J^2} &= \int dt\, \eta\, \boldsymbol{J}(\boldsymbol{x}_{ijk}, t)^2 \\
&\approx \frac{1}{2} \left(\boldsymbol{J}^2_{ijk;\, before} + \boldsymbol{J}^2_{ijk;\, after} \right) \qquad (11)
\end{aligned}
$$

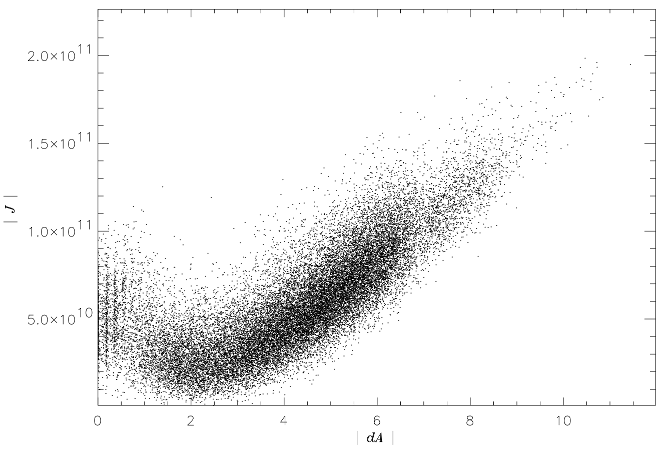

Fig. 4. Plot of the magnitude of the current $|\boldsymbol{J}_{ijk}|$ vs. the LH91 stress measure $|d\boldsymbol{A}_{ijk}|$, using the corresponding values in the whole grid at a time fixed in a loading phase in the SOC state, together with the values at bursting sites during an avalanche.

and finally, we monitor the change in magnetic energy due to a burst using the difference in magnetic energy in the local neighbourhood,

$$E_{burst}^{\Delta\boldsymbol{B}^2} = \sum_{n.n.} \left(\frac{\left(\boldsymbol{B}^{(before)}(\boldsymbol{x}_{n.n.})\right)^2}{8\pi} - \frac{\left(\boldsymbol{B}^{(after)}(\boldsymbol{x}_{n.n.})\right)^2}{8\pi} \right). \quad (12)$$

(In Eqs. (10), (11), (12), we assume $\Delta h = 1$ and $\Delta t = 1$ for the grid-spacing Δh and the time-step Δt, since, according to Isliker et al. (1998), in the classical CA models both values are not specified and set to one.)

The corresponding distributions of total energy and peak-flux are shown in Fig. 3, together with the distributions yielded by the energy-release formula of LH91, Eq. (6) (the duration distribution remains the same as in the classical LH91 model, namely a power-law, and is not shown). Obviously, the four ways of defining the released energy give basically similar results, with larger deviations only at the low and high energy ends (note that the energy in Fig. 3 is in arbitrary units). Using the formula of Ohmic dissipation does thus not change the results of the classical LH91 model.

With an estimate of the numerical value of the anomalous resistivity and of the typical size of a diffusive region or the typical diffusive time, it would be possible to introduce physical units. We did not undertake this, since all three parameters are still known only with large observational and theoretical uncertainties.

3.1.4. The relation of $d\boldsymbol{A}$ to $\boldsymbol{J}$

From the similarity of the distributions of the extended model with the ones of the classical LH91 model (Fig. 3), and from Fig. 2, where it was seen that an instability is accompanied by an enhanced current, we are led to ask directly for the relation of $d\boldsymbol{A}$ to $\boldsymbol{J}$, which we plot as a function of each other in Fig. 4. Obviously, the two quantities are related to each other: above $|d\boldsymbol{A}| \approx 2$, the current is an approximate linear function of the stress, around $|d\boldsymbol{A}| \approx 2$ the current is zero, and below there is again an approximate linear relationship, with negative slope, however (above $|d\boldsymbol{A}| \approx 2$ the current $\boldsymbol{J}$ is actually preferably along $(1, 1, 1)$, whereas below it is preferably along $(-1, -1, -1)$, i.e. $\boldsymbol{J}$ is an approximatly linear function of $d\boldsymbol{A}$ in the whole range, it merely changes its directivity at $|d\boldsymbol{A}| \approx 2$ with respect to $d\boldsymbol{A}$). In Appendix C, we show analytically why with our set-up a more or less close relation between $d\boldsymbol{A}$ and $\boldsymbol{J}$ has to be expected.

Of particular interest in Fig. 4 is that if $|d\boldsymbol{A}|$ is above the threshold $A_{cr} = 7$, then $|\boldsymbol{J}|$ is also reaching high values: obviously, large values of $|d\boldsymbol{A}|$ imply large values of $|\boldsymbol{J}|$. This confirms the statement made above: The extended CA models can be considered as models for energy release through current dissipation. It also explains why the energy distributions remain very similar when the LH91 formula for the amount of energy released in a burst ($\sim d\boldsymbol{A}^2$, Eq. (6)) is replaced by Ohmic dissipation ($\sim \boldsymbol{J}^2$, Sec. 3.1.3): bursts occur only for large stresses $|d\boldsymbol{A}|$, where $|\boldsymbol{J}|$ is also large and an approximate linear function of $|d\boldsymbol{A}|$, so that the distributions of $d\boldsymbol{A}^2$ and $\boldsymbol{J}^2$ can be expected to be the same in shape.

3.2. Application to loading with power-law increments

Georgoulis and Vlahos (1996, 1998) introduced power-law distributed increments for the loading. The main result of such a way of driving the system is that the power-law indices of the energy-distributions depend on the power-law index of the distribution of the loading increments, explaining thus the observed variability of the indices through the variability of the intensity of the driving. We generalize their way of power-law loading, which is for a scalar primary field, to a vector field in the following way: The anisotropic directivity of the loading increment $\delta\boldsymbol{A}$ is kept (see Sec. 2.1), but $|\delta\boldsymbol{A}|$ is now distributed according to

$$p(|\delta\boldsymbol{A}|) = C|\delta\boldsymbol{A}|^{-\beta} \quad (13)$$

with $|\delta\boldsymbol{A}| \in [0.01, \infty]$ and β, the power-law index, a free parameter. Simulations were performed for $\beta = 1.8$ and $\beta = 2.3$. Interested in global features implied by the CA model, our concern here is the structure of the magnetic field. It turns out that the magnetic field exhibits still a large scale organization, which is very similar to the one of the $\boldsymbol{B}$-field of the (extended with our set-up) LH91 model (Fig. 1(b)): for $\beta = 1.8$, the respective plots are visually indiscernible, and for $\beta = 2.3$ the overall shape is still roughly the same, it merely seems slightly more distorted. Thus, though the statistical results depend on β, the strength and variability of the loading, the structure of the magnetic field remains approximately the same as

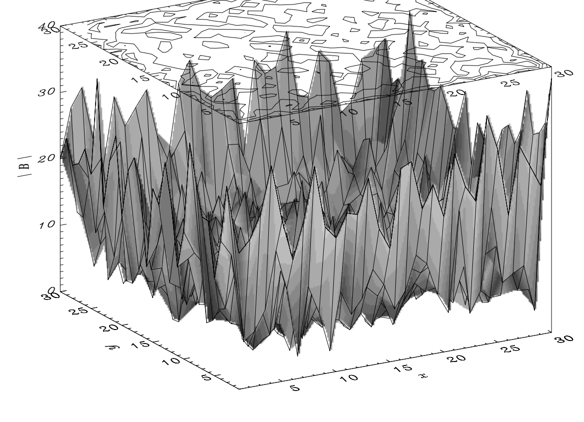

Fig. 5. Surface and contour plot of the magnitude of the the magnetic field ($|\boldsymbol{B}|$) as a function of x and y at a cut $z = 15$ through the grid, for the case of anisotropic redistribution rules.

in the case of the extended model of LH91. Large-scale organization (in the characteristic form of Fig. 1) must consequently be considered as an inherent property of SOC state, * **through the mechanism explained in Sec. 3.1.1** *.

3.3. Application to anisotropic bursts

Vlahos et al. (1995) introduced anisotropic bursts for solar flare CA models, which lead only to small events, but yield a steep distribution at small energies, predicting thus a significant over-abundance of small events with a significant contribution to coronal heating. We have first to generalize the anisotropic evolution rules, which are again for a scalar primary field, to the case of a primary vector field. A natural generalization would be to apply the anisotropic rules to the absolute magnitude of $\boldsymbol{A}$, but it turns out that this causes the algorithm to get trapped in infinite loops (two neighbouring grid-sites trigger each other mutually for ever). The same holds if we apply the anisotropic rules to the absolute magnitudes of the three components of $\boldsymbol{A}$ independently. We finally applied the anisotropic rules to the three components of $\boldsymbol{A}$ directly, not using absolute magnitudes, as also Vlahos et al. (1995) did not use absolute magnitudes, and this turned out to lead to a stationary asymptotic state: The anisotropic stress in the x-component is thus defined as

$$dA^{(x)}_{ijk;n.n.} := A^{(x)}_{ijk} - A^{(x)}_{n.n.}, \tag{14}$$

where $n.n.$ stands for one of the six nearest neighbours. The instability criterion is

$$dA^{(x)}_{ijk;n.n.} > A_{cr.} \tag{15}$$

and the redistribution rules become

$$A^{(x)}_{ijk} = A^{(x)}_{ijk} - \frac{6}{7} A_{cr.} \tag{16}$$

for the central point and

$$A^{(x)}_{n.n.} = A^{(x)}_{n.n.} + \frac{6}{7} A_{cr.} \frac{dA^{(x)}_{ijk;n.n.}}{\sum'_{n.n.} dA^{(x)}_{ijk;n.n.}}, \tag{17}$$

for those nearest neighbours which fulfill the instability criterion (Eq. 15), where the primed sum is over those neighbours for which Eq. (15) holds. The rules for $A^{(y)}, A^{(z)}$ are completely analogous (so that actually there are 18 possibilities to exceed the threshold (Eq. 15) at a given site). The released energy is assumed to amount to

$$E^{(aniso)}_{rel} = \sum_{s=x,y,z} (A^{(s)}_{ijk} - \frac{6}{7} A_{cr.})^2. \tag{18}$$

We performed a run where only the anisotropic burst-rules were applied, in order to isolate their effect, although the anisotropic burst-rules are used always together with the isotropic ones by Vlahos et al. (1995), since alone they cannot explain the complete energy distributions of flares. In Fig. 5, the magnitude of the magnetic field at a cut through the grid is shown (fixed z), for an arbitrary time (in the loading phase) during the asymptotic stationary state of the model. Clearly, there is no overall large scale structure anymore, except that the magnetic field along the boundaries is increased. The magnetic field topology is thus nearer to the concept of a random, relatively unstructured magnetic field than the magnetic field topology yielded by the isotropic models in SOC state.

* **The anisotropic burst rules do not yield large-scale structures, as they are, when used alone, also not able to lead the system to SOC state: this is obvious from the energy distributions they yield, which are much smaller in extent than the ones given by the isotropic rules (see Vlahos et al. 1995), and confirmed by the result of Lu et al. (1993) that isotropy of the redistribution rules — at least on the average — is a prerequisite to reach SOC state, at all. The anisotropic bursts occur independently in all directions and are in this way not able to organize the field in a neighbourhood systematically, and, as a consequence, also not in the entire grid.** *

The inquiry of the relation of the energy release formula Eq. (18), which is different from the isotropic formula (Eq. 6), to MHD based formulae we leave for a future study. We just note that the distributions the anisotropic model in our vector-field version yields are at lower energies, smaller in extent, and steeper than the ones of the isotropic models.

4. Summary and Conclusions

4.1. Summary

We have introduced a new set-up for classical solar flare CA models which yields, among others, consistency with

Maxwell's equations (e.g. divergence-free magnetic field), and availability of secondary variables such as currents and electric fields in accordance with MHD. Both are new for solar flare CA models. The set-up specifies the so far open physical interpretation of the CA models. This specification is to some extent unavoidably arbitrary, and it would definitely be interesting to see what alternative interpretations would yield — if they can be derived consistently. We can claim, however, that the interpretation we chose is reasonable, it is well-behaved in the sense that the derivatives of analytically prescribed vector-potentials are reproduced and that the abstract stress-measure of the CA models is related to the current, due to general properties of spline interpolation. The central problem which was to solve is how to calculate derivatives in a CA model, i.e. how to continue the primary grid-variable in-between the grid sites, since the notion of derivatives is alien in the context of CA models quite in general.

In this article, our main aim with the introduced set-up was to demonstrate that the set-up truly extends the classical CA models and makes them richer in the sense that they contain much more information, now. The main features we revealed about the CA models, extended with our set-up, are:

1. Large-scale organization of the vector-potential and the magnetic field: The field topology during SOC state is bound to characteristic large-scale structures which span the whole grid, very pronounced for the primary grid variable, the vector-potential, but also for the magnetic field. Bursts and flares are just slight disturbances propagating over the large-scale structures, which are always maintained, also in the largest events. The magnitude of the current, as a second order derivative of the primary field, does not show any obvious large-scale structure anymore, it reflects more or less only the random fluctuations of the large-scale organized magnetic field. It is worthwhile noting that the large-scale structure of the primary grid-variable is not an artificial result of our set-up, but a ***natural*** consequence of the SOC state in which the system finds itself. The appearance of large-scale structures for the primary grid variable was ***shown*** here for the first time. It may have been known to different authors, but it never has explicitly been shown: SOC models for flares are derived in analogy to sand-pile dynamics, and the paradigm of a pile reappears in the field topologies of the solar flare CA models.

2. Increased current at unstable grid-sites: Unstable sites are characterized by an enhanced current, which is reduced after a burst has taken place, as a result of which the current at a grid-site in the neighbourhood may be increased.

3. Availability of the electric field: The electric field is ***approximated*** with the resistive part of Ohm's law ***in its simple form***, which can ***in general*** be expected to be a good approximation in ***coronal*** applications and where the interest is in current-dissipation events, e.g. in the case of solar flares.

4. Energy release in terms of Ohmic dissipation: We replaced the some-what *ad hoc* formula in the CA models to estimate the energy released in a burst with the expression for Ohmic dissipation in terms of the current. The distributions yielded in this way are very similar to the ones based on the ad hoc formula, so that the results of the CA models remain basically unchanged.

5. CA as models for current dissipations: As a consequence of point 2 and 4 in this list, and of the fact that there is an approximate linear relation between the current and the stress measure of the CA, we can conclude that the *extended* CA models can be considered as models for energy release through current dissipation.

4.2. Conclusions

Our set-up is to be contrasted to the recently suggested MHD-derived (not based on the sand-pile analogy) CA models of Einaudi & Velli (1999), MacPherson & MacKinnon (1999), Longcope and Noonan (2000), and Isliker et al. (2000a). They all suggest new evolution rules, derived from MHD, and all in different ways (they actually focus on different processes, namely the microscopic, macroscopic, and mesoscopic physics, respectively, in active regions). Our set-up, on the other hand, uses existing CA models, does not interfere (if not wished) with their evolution rules, does also not change their main results, as shown, but reinterprets them, extends them essentially, and makes them compatible with MHD.

The set-up we introduced allows different future applications and posing questions which could not be asked so far in the frame of CA models. In preparation is a study (Isliker et al. 2000b) to reveal in detail what physical flare scenario the extended CA models imply. We will address the questions: (1) how to interpret the small scale processes of the models (loading and bursting) in terms of MHD; (2) what the *global* flare-scenario implied by the models is; (3) whether the global magnetic field topology of the models can be considered to represent observed magnetic topologies in active regions; (4) what spatio-temporal evolution of the electric field during flares is yielded by the models.

A different future application we plan with CA models extended with our set-up is the introduction of particles into the models, with the aim to study thermal emission, particle acceleration, and non-thermal emission. This will allow a much deeper comparison of the CA models to observations than was possible so far, and this is actually the most important benefit of the set-up we introduced. Such comparisons will allow a new judgment of the adequateness or not of classical CA models (in their current form) to the problem of solar flares, beyond the three statistical distributions of the primarily released energy. Solar flare

CA models which include particle acceleration would represent the first global and complete model for solar flares.

Acknowledgements. We thank K. Tsiganis and M. Georgoulis for many helpful discussions on several issues. We also thank G. Einaudi for stimulating discussions on MHD aspects of flares, and the referee A.L. MacKinnon for useful comments. The work of H. Isliker was partly supported by a grant of the Swiss National Science Foundation (NF grant nr. 8220-046504).

Appendix A: Temporal evolution of the CA

The temporal evolution of the CA models presented in this article is governed by the following rules:

0. initializing
1. loading
2. scanning: create a list of the unstable sites; if there are none, return to loading (1)
3. scanning and bursting: redistribute the fields at the unstable sites which are in the list created in the scannings 2 or 4
4. scanning: create a list of the unstable sites. If there are any, go to bursting (3), else return to loading (1)

The extra scannings 2 and 4 are needed for causality: if a site becomes unstable through a burst in the neighbourhood, then it should be redistributed in the subsequent scan, and not in the same as the primary unstable site. The same is true for the scanning 4, since in the next bursting phase (if any) only those sites should burst who had become unstable through a burst in their neighbourhood during the foregoing time-step.

As a time-step is considered one scanning of the grid, point 3. The released energy per time-step is the sum of all the energy released by bursts in this time-step (a burst is considered a single redistribution event in 3). We term a flare or avalanche the loop 3,4, from the occurring of the first burst in 3 until the activity has died out and one returns via the scanning 4 to loading (1). The duration of the flare is the number of time-steps it lasted, the total flare energy is the sum of all the energies released in the duration of the flare, and the peak flux or peak energy is the maximum of the energies of all the time-steps of the flare.

Appendix B: Why spline interpolation is particularly adequate: comparison to other methods of continuation

We mentioned in Sec. 2.2 that other possibilities for continuation of the vector-potential besides spline interpolation would be: a) continuation of $\boldsymbol{A}$ with the help of an equation; b) other kinds of interpolation, either locally (in a neighbourhood), or globally (through the whole grid). Possibility a) implies that an equation has to be solved in each time-step (after each loading and after each burst), in the worst case numerically, with ***open*** boundary condition and the $\boldsymbol{A}_{ijk}$ ***given*** at the grid-sites. This computational effort might slow down the algorithm of the model considerably (and bring it near to the computational effort of MHD equation integration). Besides that, the problem is what equation to use: to make the magnetic field always a potential field (i.e. using a corresponding equation for the vector-potential $\boldsymbol{A}$) implies that, from the point of view of MHD, at all times a very 'well-behaved' magnetic field resides in the CA, with no tendency towards instabilities, which makes it difficult to understand why bursts should occur at all, since critical quantities such as currents do not become excited. A better candidate could be expected to be force-freeness, except that, possibly, one may be confronted with incompatibility of the boundary conditions with the vector-potential values given at the grid-sites, i.e. existence-problems for solutions eventually arise.

Though definitely possibility a) cannot be ruled out on solid grounds, we found it more promising to proceed with possibility b), interpolation. A guide-line for choosing a particular interpolation method is the reasonable demand that the interpolation should not introduce wild oscillations in-between grid-sites, for we want to assure that the derivatives at the grid sites, which are very sensitive to such oscillations, are not 'random' values solely due to the interpolation, but that they reflect more or less directly the change of the primary grid-variable from grid-site to grid-site. This calls for interpolating functions which are as little curved as possible.

The easiest and fastest way of interpolating would be to perform local interpolations around a point and its nearest neighbours (e.g. using low-order polynomials or trigonometric functions of different degrees). This interpolation leads, however, to ambiguities for the derivatives: the derivatives, say at a point $\boldsymbol{x}_{ijk}$, are not the same, if the used interpolation is centered at $\boldsymbol{x}_{ijk}$, with the ones calculated with an interpolation centered at e.g. $\boldsymbol{x}_{i+1jk}$. In this sense, local interpolation is not self-consistent, the derivatives at a grid-site depend on where the used interpolation is centered.

Finally, we are left with global interpolation through the whole grid. Among the candidates are, besides more exotic interpolating functions, polynomials of degree equal to the grid size, trigonometric functions (also in the form of Fourier-transforms), low-order smooth polynomials (e.g. splines). The first candidate, polynomials of a high degree n (with n the number of grid points in one direction), we reject immediately since it is notorious for its strong oscillations in-between grid-sites, mainly towards the edges of the grid. We tried the second candidate, trigonometric interpolation, in the form of discrete Fourier transform. Testing this by prescribing analytic functions for $\boldsymbol{A}(\boldsymbol{x})$ and comparing the numerical derivatives with the analytic ones, it turned out that there arise problems with representing structures in $\boldsymbol{A}$ as large as the entire grid (the wave-number spectrum is too limited), and with structures as short as roughly the grid-spacing (different prescribed short structures are taken for the same).

Trying cubic spline-interpolation, we found that it does not suffer from the problems stated for the other types of interpolation: neither does it introduce wild oscillations, unmotivated by the values at the grid-sites, nor does spline interpolation have problems with describing large or small scale structures (if a functional form of $\boldsymbol{A}$ is prescribed, then the analytic derivatives and the derivatives yielded by the interpolation give very close values, in general).

Moreover, based on results of Sec. 3, App. C, and Isliker et al. (1998), there is another reason why spline-interpolation is particularly adequate to our problem: It relates the quantity $d\boldsymbol{A}$ (Eq. (2)), which measures the stress at a site in the CA model, closely to $\nabla^2\boldsymbol{A}$, the Laplacian of $\boldsymbol{A}$ (see App. C). The latter is related to the current ($\boldsymbol{J} = -\frac{c}{4\pi}\nabla^2\boldsymbol{A} + \frac{c}{4\pi}\nabla(\nabla\boldsymbol{A})$), which, from the point of view of MHD, can be considered as a measure of stress in the magnetic field configuration. If this relation would not hold, then the redistribution rules (Eqs. (4) and (5)) of the CA would not be interpretable as the diffusion process revealed by Isliker et al. (1998), and the instability criterion (Eq. 3) would not be so closely related to the current (see Sec. 3 and App. C).

B.1. Why in particular differencing is not adequate to calculate derivatives in a CA

We had rejected above (Sec. 1, Sec. 2.2) the use of difference expressions to calculate derivatives, stating that differencing is not in the spirit of CA models quite in general, since the nature of CA is truly discrete. We think it worthwhile to make this argument more concrete and to show what problems arise if differencing were used:

1. Consistency with the evolution rules: Isliker et al. (1998) have shown that the classical solar flare CA are not just the discretized form of a differential equations. Instead, they describe the time-evolution of a system by rules which express the direct transition from a given initial to a final state which is the asymptotic solution of a simple diffusion equation. The time-step corresponds therewith to the average time needed for smallest scale structures (structures as large as a neighbourhood) to diffuse, and the grid-size corresponds to the size of these smallest occurring structures. Assuming that the CA models were just discretized differential equations would lead to severe mathematical and physical contradictions and inconsistencies (continuity for $\Delta h \to 0$ is violated (with Δh the grid-size), and negative diffusivities appear). Therewith, in order to be consistent with the evolution rules, which assume a finite grid-size, one cannot assume for the purpose of differentiating this same grid-size to be approximately infinitesimal.

2. Derivatives as difference expressions are not self-consistent: There are several equivalent ways to define numerical derivatives with the use of difference expressions: there are e.g. the backward difference $\partial_x A_x(\boldsymbol{x}_{ijk}) = (A_x(\boldsymbol{x}_{ijk}) - A_x(\boldsymbol{x}_{i-1jk}))/\Delta h$, and the forward difference $\partial_x A_x(\boldsymbol{x}_{ijk}) = (A_x(\boldsymbol{x}_{i+1jk}) - A_x(\boldsymbol{x}_{ijk}))/\Delta h$. Both should give comparable values in a given application, else, in the context of differential equation integration, one would have to make the resolution higher. In the case of CA-models, we find that the two difference expressions yield values which differ substantially from each other: E.g. for an initial loading of the grid with independent random values for the $\boldsymbol{A}$-field, the difference between the backward and the forward difference expression can be as large as the field itself. Such an initial condition would of course not make sense in the context of partial differential equations, in the context of CA, however, it is a reasonable starting configuration, and the evolution is unaffected by such an initial loading. Moreover, when the CA models we discuss in this article have reached the SOC state, then the differences between e.g. the backward- and forward-difference expressions can be as large as 400%. There is no way to reduce this discrepancy, since grid-refinement is principally impossible for CA: the evolution is governed by a set of rules, and making the grid spacing smaller by introducing new grid-points in-between the old ones would actually just mean to make the grid larger, since the evolution rules remain the same, there are no rules for half the grid-spacing.

Appendix C: Relation of dA to ΔA

The stress measure of LH91, $d\boldsymbol{A}_{ijk} = \boldsymbol{A}_{ijk} - \frac{1}{6}\sum_{n.n.}\boldsymbol{A}_{n.n.}$, can be related to continuous expressions by representing the values of $\boldsymbol{A}_{n.n.}$ as Taylor-series expansions around $\boldsymbol{x}_{ijk}$, setting the spatial differences to $\Delta h = 1$. It turns out that e.g.

$$dA_z = -\frac{1}{6}\Delta A_z - \frac{1}{72}(\partial_x^4 + \partial_y^4 + \partial_z^4)A_z - ... \quad \text{(C.1)}$$

and so on for the other two components. *In general,* it is therefore *not* adequate to consider $d\boldsymbol{A}$ to be a good 4th order approximation to $\Delta\boldsymbol{A}$, since higher order corrections can be large, they depend on the way the vector potential is continued in-between grid-sites. If we had, for instance, chosen global polynomial interpolation instead of spline-interpolation, the higher order terms would not be negligible, above all towards the edges of the grid, since polynomial interpolation is known for introducing fluctuations near the edges of the grid. Consequently, $d\boldsymbol{A}$ would be a bad approximation to $\Delta\boldsymbol{A}$. In order $d\boldsymbol{A}$ to be a good approximation to $\Delta\boldsymbol{A}$, interpolation with, for example, 3rd order polynomials would be an optimum choice ($d\boldsymbol{A}$ would be an exact approximation to $\Delta\boldsymbol{A}$). Thus, 3rd order polynomials would be the choice for local interpolation, which, however, is not applicable, since it introduces discontinuities in $\boldsymbol{B}$ and $\boldsymbol{J}$ (see App. B). The way out of the dilemma we suggested in this article is the use of cubic splines, which provide global interpolation with 3rd order polynomials, with $\boldsymbol{B}$ and $\boldsymbol{J}$ continuous, and only third order derivatives are discontinuous (this is the price of the compromise). For splines then, Eq. (C.1) writes as

$$dA_z = -\frac{1}{6}\Delta A_z - \frac{1}{36}\Big[\; (\;\partial_x^3 A_z^+ - \partial_x^3 A_z^-)+ \\ (\;\partial_y^3 A_z^+ - \partial_y^3 A_z^-)+ \\ (\;\partial_z^3 A_z^+ - \partial_z^3 A_z^-)\Big], \qquad \text{(C.2)}$$

due to the discontinuities in the 3rd order derivatives (the superscripts $+$ and $-$ refer to the right and left derivative, respectively). Thus, in case where the third order right and left derivatives are not too different, $d\boldsymbol{A}$ is a good approximation to $\Delta\boldsymbol{A}$.

References

Bak, P., Tang, C., Wiesenfeld, K., 1987, Phys. Rev. Lett. 59, 381

Bak, P., Tang, C., Wiesenfeld, K., 1988, Phys. Rev. A 38, 364

Bromund, K. R., McTiernan, J. M., Kane, S. R., 1995, Ap. J . 455, 733

Dmitruk, P., Gomez, D.O., 1998, Ap. J. 505, 974

Einaudi, G., Velli, M., Politano, H., Pouquet, A., 1996, Ap. J. 457, L13

Einaudi, G., Velli, M., 1999, Physics of Plasmas 6 (No. 11), 4146

Galsgaard, K., 1996, A&A 315, 312

Galsgaard, K., Nordlund, A., 1996, J. Geophys. Res. 101, 13445

Galtier, S., Pouquet, A., 1998, Sol. Phys. 179, 141

Georgoulis, M., Velli, M., Einaudi, G., 1998, Ap. J. 497, 957

Georgoulis, M., Vlahos, L., 1996, Ap. J. 469, L135

Georgoulis, M., Vlahos, L., 1998, A&A 336, 721

Hendrix, D.L., Van Hoven, G., 1996, Ap. J. 467, 887

Isliker, H., Anastasiadis, A., Vassiliadis, D., Vlahos, L., 1998, A&A, 335, 1085

Isliker, H., Anastasiadis, A., Vlahos, L., 2000a, 'A solar flare model in between MHD and Cellular Automaton', in The Fourth Astronomical Conference of The Hellenic Astronomical Society, eds. Seimenis, J. et al., in press

Isliker, H., Anastasiadis, A., Vlahos, L., 2000b, A&A, to be submitted

Longcope, D.W., Noonan, E.J., 2000, Ap. J., in press

Longcope, L., Sudan, L., 1994, Ap. J. 437, 491

Lu, T.E., Hamilton, R.J., 1991, Ap. J. 380, L89 [LH91]

Lu, T.E., Hamilton, R.J., McTiernan, J.M., Bromund, K.R., 1993, Ap. J. 412, 841

MacPherson, K.P., MacKinnon, A.L., 1999, A&A 350, 1040

Mikic, Z., Schnack, D.D., Van Hoven, G., 1989, Ap. J. 338, 1148

Parker, E.N., 1993, Ap. J. 414, 389

Press, W.H., Teukolsky, S.A., Vetterling, W.T., Flannery, B.P., 1992, Numerical Recipes in Fortran, 2nd ed. (Cambridge University Press, Cambridge)

Strauss, H., 1993, Geophys. Res. Lett. 20, 325

Vassiliadis, D., Anastasiadis, A., Georgoulis, M., Vlahos, L., 1998, Ap. J. 509, L53

Vlahos, L., Georgoulis, M., Kluiving, R., Paschos, P., 1995, A&A 299, 897